

Metal-Poor Stars in the MW Disk: Resonant Cooling of Vertical Oscillations of Halo Stars in Barred Galaxies

XINGCHEN LI ¹ ISAAC SHLOSMAN ^{1,2} DANIEL PFENNIGER ³ AND CLAYTON HELLER ⁴

¹*Department of Physics & Astronomy, University of Kentucky, Lexington, KY 40506, USA*

²*Theoretical Astrophysics, School of Sciences, Osaka University, Osaka 560-0043, Japan*

³*University of Geneva, Geneva Observatory, ch. Pegasi 51, 1290 Versoix, Switzerland*

⁴*Department of Biochemistry, Chemistry & Physics, Georgia Southern University, Statesboro, GA 30460, USA*

ABSTRACT

Using numerical simulations of a barred disk galaxy embedded in nonspinning and spinning dark matter (DM) halos, we present a novel mechanism of ‘cooling’ the vertical oscillations of halo DM particles, which acquire the disk kinematics. The underlying mechanism consists of resonant interactions between halo particles and the stellar bar. The cooling mechanism acts both on dynamical and secular timescales, i.e., from ~ 0.5 Gyr to few Gyr, and the stellar bar acts to absorb the kinetic energy of the vertical motions. Using a Milky Way-type stellar halo, we estimate the population of metal-poor disk stars which have been trapped by the MW disk and analyze its kinematics. We find that the population of metal-poor MW disk stars with $|z| \lesssim 3$ kpc detected by the Gaia DR3 and other surveys can have their origin in the stellar halo. The cooled population also migrates radially outwards compared by acquiring energy from the spinning bar, and prograde-moving stars have a different distribution from the retrograde ones. Next, we have calculated the ratio of the prograde-to-retrograde orbits of the cooled population and found that this ratio varies radially, with the fast-spinning stellar halo resulting in the shallower radial increase of this ratio outside of the corotation. The nonspinning stellar halo shows a monotonic increase of this ratio with radius outside the corotation. Together with analyzed radial migration of these halo stars, the cooling phenomenon of halo metal-poor stars can explain their current disk population, and has corollaries for chemical evolution of disk galaxies in general.

Keywords: Galaxy dynamics(591) — Galaxy bars(2364) — Galaxy disks(589) — Galaxy evolution(594)
— Galaxy formation(595)

1. INTRODUCTION

Recent observations have detected a population of low metallicity stars with $[\text{Fe}/\text{H}] \leq -2.5$ dex in the Milky Way (MW) stellar disk. About 31% of these stars reside in the galactic disk, within $|z| \leq 3$ kpc of its midplane (e.g., Sestito et al. 2020; Lucey et al. 2021). The *Pristine* photometric survey (Starkenburg et al. 2017), Hamburg/ESO (Reimers 1990; Beers et al. 1999) and Gaia EDR3 (Gaia Collaboration et al. 2021) surveys have quantified some of the properties of this population. Moreover, this population appears to be statistically biased to populate prograde orbits with respect to the disk rotation. Bellazzini et al. (2023) have analyzed the metal-poor stars in the Solar neighborhood and found that among the disk kinematics, the ratio of the prograde to retrograde orbits is $\sim 3/1$. Finally, Zhang et al. (2023) have analyzed the Gaia DR3 kinematic sample of the metal-poor population in the MW and found two kinematic groups — one stationary and one with a net prograde rotation of 80 km s^{-1} .

Several suggestions have been made to the origin of these metal-poor stars in the disk. It can come from the early buildup of the MW, especially stars on the retrograde orbits, and from minor mergers (e.g., Sestito et al. 2021; Carollo et al. 2023). Metal-poor disk stars also appear on very eccentric orbits. Other suggestions include the early formation

of the metal-poor stars entirely in the MW disk that is heated to form a thick disk (e.g., Di Matteo et al. 2020). Or they could be shepherded by the stellar bar, i.e., trapped by its corotation resonance from the inner galaxy (e.g., Yuan et al. 2023).

Here, we analyze a new process which affects the halo population, moving a small fraction of this population into the stellar disk, and propose a novel scenario for the origin of the observed low metallicity stellar population confined close to the mid-plane of the MW and other disk galaxies. The majority of disk galaxies host stellar bars on various spatial scales (e.g., Sellwood & Wilkinson 1993; Knapen et al. 2000; Jogee et al. 2004). These systems have been modeled extensively using 3-D numerical simulations, and many of their properties have been successfully analyzed (e.g., Sellwood 1980; Athanassoula et al. 1983; Pfenniger 1984; Weinberg 1985; Combes et al. 1990; Raha et al. 1991; Athanassoula 2003; Martinez-Valpuesta et al. 2006; Dubinski et al. 2009; Villa-Vargas et al. 2009; Bi et al. 2022). Nevertheless, these collisionless systems continue to provide new effects, such the effect of spinning DM halos and bulges (e.g., Long et al. 2014; Collier et al. 2018; Li et al. 2023b; Li et al. 2023c). We define the DM halo spin as $\lambda = J/J_{\text{max}}$ following Bullock et al. (2001), where J is the halo angular momentum and J_{max} is maximally allowed J .

Interactions between the stellar population of galactic disks and galactic bars have been studied extensively and are dominated by resonances. These interactions include resonances between the orbits in the disk plane and those in the vertical plane have been found to be associated with the energy transfer from the disk motions to the vertical motions (Friedli & Pfenniger 1990; Combes et al. 1990; Li et al. 2023a). More generally, one expects that interactions between the DM halo population and the embedded barred stellar disks involve resonances between halo orbits and stellar bars. In this work, we highlight one of such resonant effects which leads to the cooling of vertical stellar oscillations in spinless and spinning halos. We limit ourselves to the outcomes of this effect — the origin of disk metal-poor stars. In the follow-up work, we will take a more comprehensive look at halo-disk resonances.

Collisionless systems, such as galaxies or DM halos exchange their energies on a timescale which is much longer than the Hubble time. Their relaxation in this process characterized by small angle encounters, i.e., essentially two-body distant collisions, can be described using the Fokker-Planck equation (e.g., Binney & Tremaine 2008). The alternative to this relaxation is the evolution (i) in a time-dependent gravitational potential, when the individual energies of particles are not conserved and can be exchanged with the mean field (Lynden-Bell 1967), or (ii) by resonant interactions. The former evolution does not lead to the Maxwellian distribution of velocities, while the end-process of the latter interaction is less clear.

In this work, we use two standard models, with $\lambda = 0$ and 0.06, in order to demonstrate an interesting effect, which so far has eluded the attention of modelers and theorists. The higher value of λ has been selected based on the first measurement of the MW DM halo spin, $\lambda \sim 0.061 - 0.088$ (Obreja et al. 2022). Section 2 describes the numerical models, section 3 presents our results, and section 4 analyzes these results and discusses their implications for galaxy evolution.

2. NUMERICAL METHODS

We use the N -body part of the mesh-free hydrodynamics code GIZMO (Hopkins 2015), an extension of the GADGET-2 code (Springel 2005). The models of stellar disk galaxies embedded in spherical DM halos have been constructed with two different halo spins using methods described elsewhere (e.g., Collier et al. 2018; Li et al. 2023b). We re-simulated the model with the halo virial radius of 180 kpc from Li et al. (2023b) with $\lambda = 0$ and $\lambda = 0.06$, using $N_{\text{DM}} = 7.2 \times 10^6$ DM particles and $N_{\text{S}} = 8 \times 10^5$ stellar particles. The mass-per-particle in the disk is $7.9 \times 10^4 M_{\odot}$ and $8.7 \times 10^4 M_{\odot}$ in the halo. The gravitational softening is $\epsilon = 25$ pc for each particle. The models have been run for 10 Gyr, with total angular momentum conserved within 0.2% and total energy within 0.1% over the total integration time.

The DM component has the NFW density profile (Navarro et al. 1996) relaxed in the exponential disk potential, with $r_c = 1.4$ kpc, the flat density core, and $r_s = 10$ kpc, the characteristic radius. We use a Gaussian cut-off radius $r_t = 180$ kpc to obtain a finite mass of $M_h = 6.3 \times 10^{11} M_{\odot}$. The initial exponential stellar disk has the mass $M_d = 6.3 \times 10^{10} M_{\odot}$ and radial scale-length $R_0 = 2.85$ kpc, and the scale-height $z_0 = 0.6$ kpc. Velocities of disk particles are assigned using the epicycle approximation and asymmetric drift correction (Li et al. 2023b).

Two models of DM halos are abbreviated as P00 (for $\lambda = 0$) and P60 (for $\lambda = 0.06$). The angular momentum axis of the DM halo in the P60 model agrees with that of the disk.

3. RESULTS

Both models, P00 and P60, are subject to the bar instability and their evolution is described in Li et al. (2023b) and in Figure 1, displaying the bar Fourier amplitude, A_2 , the buckling Fourier amplitude, A_{1z} , and the bar pattern speed,

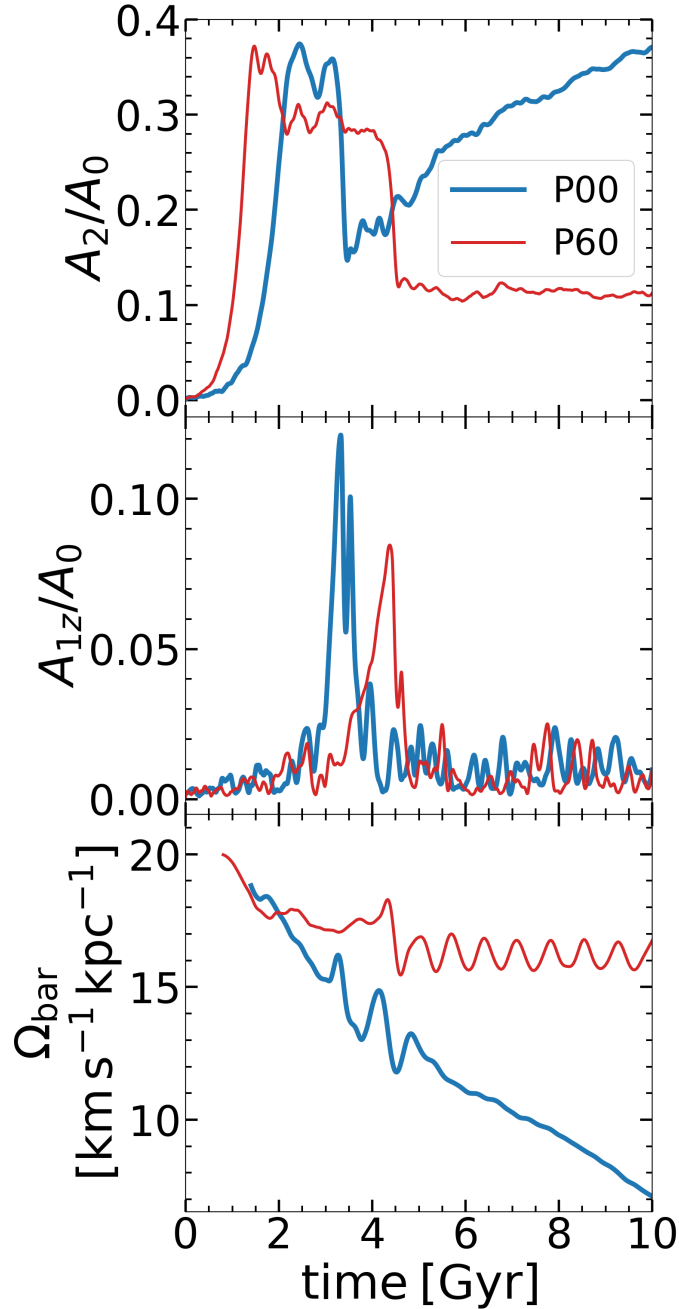


Figure 1. Evolution of the bar strength A_2 , buckling strength A_{1z} , and the bar pattern speed Ω_{bar} in the P00 (blue) and P60 (red) models.

Ω_{bar} . The stellar bar evolution depends on the halo λ . The P00 bar experiences vertical buckling at $t \sim 3.3$ Gyr, and fully re-grows after, while the P60 bar buckles at about 4 Gyr, essentially leaving behind only an oval distortion, and its torque against the DM, therefore, is very weak.

We have performed an orbit analysis [see e.g., Li et al. (2023c) for details] for both models by constructing a sample of halo particles from each model. The sampled particles have been selected as follows (see Figure 2). (1) We calculated the maximal potential Φ_{max} from the region within the cylindrical radius $R < 15$ kpc and vertical distance $|z| < 15$ kpc at $t = 0.5$ Gyr; (2) inside the equipotential surface of Φ_{max} , we randomly choose 6.5×10^5 DM particles whose specific energy is smaller than Φ_{max} .

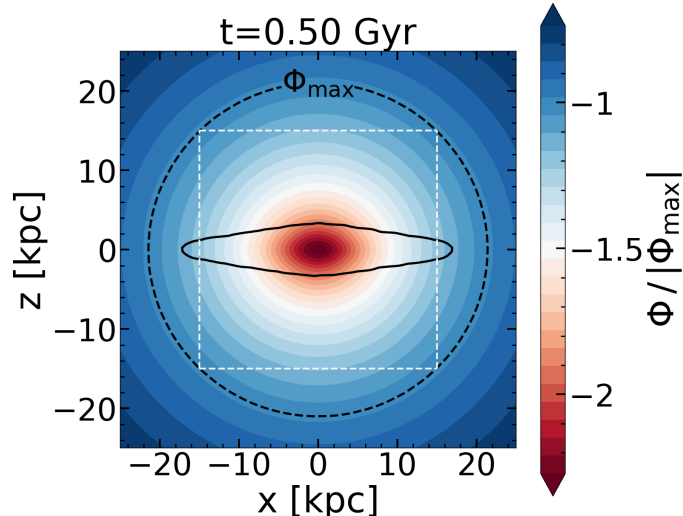


Figure 2. A schematic figure of the region where the DM particles are sampled. The Figure is in the disk plane’s edge-on view ($x - z$ plane) at $t = 0.50$ Gyr. The colored contours are the equipotential surfaces of the total system. The gray dashed box indicates the volume of a cylinder with a radius $R = 15$ kpc and vertical extension from $z = -15$ to $z = 15$ kpc. The dashed ‘circle’ is an equipotential surface with the maximal potential Φ_{\max} found inside the cylinder. The envelope of the disk is plotted as the solid black curve. We randomly sampled 6.5×10^5 DM particles inside Φ_{\max} equipotential surface whose specific energy is smaller than the Φ_{\max} .

We have determined various parameters of individual orbits of DM particles, namely, their maxima along the z -axis, z_{\max} , and along the cylindrical R -axis, R_{\max} . By focusing on the evolution of $z_{\max}(t)$, we have detected its decrease by a factor ≥ 2 over various time periods. To analyze the statistical properties of these DM particle orbits, we have binned the evolution of $z_{\max}(t)$ into time periods of $\Delta t \leq 0.5$ Gyr. We call abruptly ‘cooled’ particles those cooled over $\Delta t \leq 0.5$ Gyr, to separate them from all other cooled halo particles over longer time periods, i.e., 0.5–1.0 Gyr, 1.0–1.5 Gyr, 1.5–2.0 Gyr, and so on.

Note that the z -coordinate of each particle has been measured with respect to the Laplace surface defined by the surface where the vertical acceleration a_z vanishes (e.g., Li et al. 2023c). Next, we have calculated $\langle z_{\max} \rangle$ —the time-averaged z_{\max} for each consecutive 0.5 Gyr bin from $t = 0$ to $t = 10$ Gyr.

Figure 3 displays the typical behaviors of $\langle z_{\max} \rangle$ of cooling DM particles. Firstly, a particle cools down abruptly by a factor of ≥ 2 and never heats up again. Second, a particle cools down and heats up after some time period. Next, a particle cools down abruptly and heats up multiple times over the simulation run. Lastly, a particle cools down gradually over 8 Gyr.

To obtain the statistics of cooled halo particles, we proceed with the following definitions. First, we assume that the stellar disk extends to $z_{\text{disk}} = 3$ kpc above/below the midplane, based on the edge-on disk density contours. Second, we focus on these halo particles which acquire the disk kinematics. Third, in Section 4, we consider a fraction of cooled DM particles as the low metallicity halo stars that have obtained the disk kinematics. For this purpose, we limit our statistical analysis to DM particles with $\langle z_{\max} \rangle \geq 2z_{\text{disk}}$ only before the cooling process begins. This also explains the requirement of cooling $\langle z_{\max} \rangle$ by a factor of ≥ 2 .

We define a sub-sample of all DM halo particles that cool down from the high altitude into the disk in each bin by all types of cooling, i.e., abruptly, gradually, and multiple coolings, $N_{\text{cool}}(t)$. In both the P00 and P60 models, the particles of this sub-sample are filtered out of the total sample discussed above by imposing the two conditions: (1) $\langle z_{\max} \rangle > 2z_{\text{disk}}$ at the time of sampling ($t = 0.5$ Gyr); (2) $\langle z_{\max} \rangle < z_{\text{disk}}$, after the cooling.

The top panel of Figure 4 shows the cumulative number of cooled DM halo particles as a function of time, $N_{\text{cool}}(t)$, for each model, i.e., only the DM particles that remain in the disk. The re-heated DM particles, i.e., those leaving the disk, have been excluded. Hence, $N_{\text{cool}}(t = 10 \text{ Gyr})$ gives the number of the cooled DM particles remaining in the disk by the end of the run. The bottom panel shows the duration distribution of individual cooling events over $t = 10$ Gyr.

The sample of DM particles used to analyze the statistics of cooling events includes only the particles with $\langle z_{\max} \rangle$ larger than two times z_{disk} . This number is $N_{\text{total}} = 325,270$ for the P00 model and 325,019 for the P60 model.

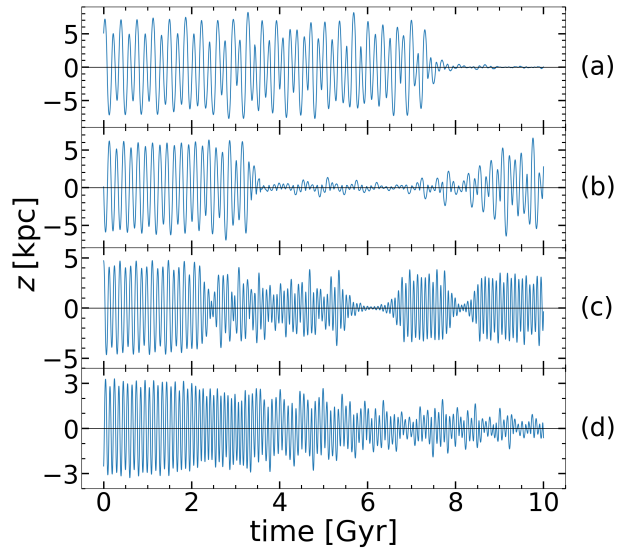


Figure 3. Four representative examples of cooling particles in the P00 model. The z -coordinate of each particle is measured with respect to the Laplace surface. (a) Abruptly cooling particle at ~ 6.5 Gyr and never heats up again until the end of the run. (b) The particle cools down abruptly at ~ 3.5 Gyr and heats up at ~ 8 Gyr. (c) The particle experiences multiple coolings at ~ 2.5 , ~ 5.8 , and ~ 8 Gyr. (d) The particle cools down gradually from ~ 2 to ~ 10 Gyr.

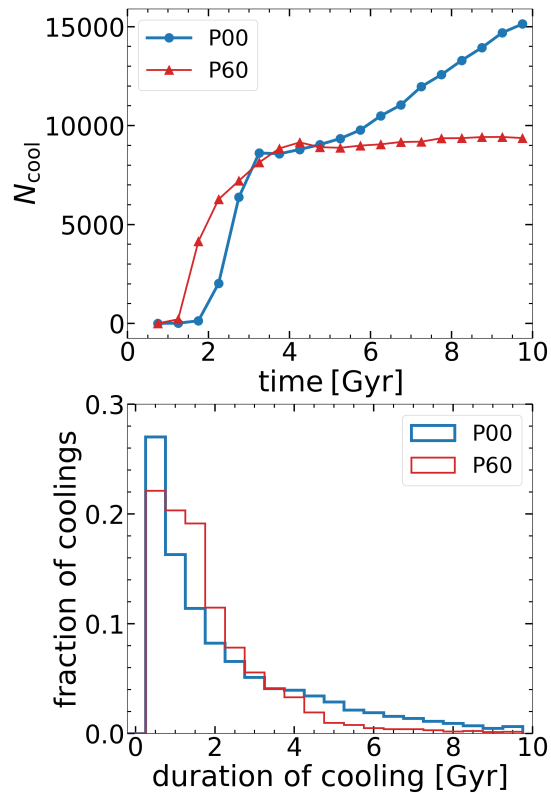


Figure 4. Statistics of a sub-sample of DM halo particles which cool down from high altitude into the disk plane. These particles are selected under two conditions (see text for details) from the P00 (blue) and the P60 (red) models. Top frame: The *net* number of sub-sampled particles whose $\langle z_{\max} \rangle$ are smaller than the disk thickness after a cooling event. Particles that are heated up and leaving the disk (i.e., $\langle z_{\max} \rangle$ larger than the disk thickness) in each time bin are excluded. *Bottom frame:* The histogram of the duration of individual cooling events for particles that are found in the disk at $t = 10$ Gyr (i.e., the particles at the end-point in the top panel).

Table 1. Statistics of cooled halo particles for P00 and P60 models at $t = 10$ Gyr and of cooled halo stars at $z = 0$. $f_{\text{cool}}(\text{abrupt})$ is the probability to find an abruptly cooled halo ‘star’ in the stellar disk moving with the disk kinematics; N_{total} is the number of halo particles with $\langle z_{\text{max}} \rangle > 2z_{\text{disk}}$ from the entire sample, N_{total} , at $t = 0.5$ Gyr; prograde/retrograde ratio of cooled down halo particles found in the disk. $N_{*,\text{cool}}(\text{total})$ is the estimated number of halo stars cooled down to the disk plane, using the Milky Way stellar halo.

	Model	P00	P60
Simulations	halo spin λ	0	0.06
	N_{total}	325,270	325,019
	$f_{\text{cool}}(\text{abrupt})$	2.9%	1.8%
	$f_{\text{cool}}(\text{total})$	4.7%	2.9%
Stellar halo	$N_{*,\text{cool}}(\text{total})$	9×10^6	5×10^6

4. DISCUSSION

We have shown that a population of halo particles that oscillate about the potential midplane, i.e., about the Laplace surface, can decrease their amplitudes of oscillations in a short time period, $\sim 2 - 3$ oscillations. In other words, they are ‘cooled down’ abruptly. Other DM halo particles cool down but over longer time periods. When associating the DM particle trajectories with those of the halo metal-poor stars, one deals with the migration of halo stars to the disk. A number of interesting corollaries emerge as a result of this new process. But first of all, what is the underlying mechanism of this migration?

We start with an analogy: imagine a population of ping-pong balls above a moving floor. Both the balls and the floor can oscillate only along the vertical coordinate z , each with a different frequency and amplitude. We assume that the ball-floor collisions are elastic and that the ball population is released at various heights above $z = 0$. Now, we analyze the results of the ball-floor collisions.

Some balls will acquire or lose kinetic energy from the collision with the floor depending on their velocity differences with the floor at the time of contact. Increasing or decreasing vertical kinetic energy is analogous to ‘heating up’ or cooling the balls, respectively. Some collisions will result in a substantial cooling of the vertical motions — this sub-population of balls will be trapped close to the floor. Some of the balls will be trapped for a prolonged time period, some will be re-heated and re-cooled multiple times. These outcomes demonstrate the possibility of the resonance cooling of the balls.

This toy model of ping pong balls – moving floor interactions can serve as a simplified analogy to vertical oscillations of halo stars and the horizontal motion of the stellar bar in the embedded galactic disk and their energy exchange. Halo stars can exchange energy and angular momentum with the spinning bar depending on their relative position before and after crossing the bar potential. As a result, the amplitude of the vertical oscillations will increase or decrease. A resonance between halo orbits and the bar perturbations leads to a fast energy transfer, i.e., during 2–3 vertical oscillations and cooling of these motions. This is the essence of the mechanism operating in barred galaxies and leading to the formation of the ‘cold’ population of metal-poor stars in the disk.

In the P00 model, $\sim 2.67 \times 10^5$ abrupt coolings happened for $\sim 1.84 \times 10^5$ DM particles. In the P60 model, $\sim 1.54 \times 10^5$ abrupt coolings happened for $\sim 1.05 \times 10^5$ DM particles. Figure 5 displays additional statistics of the *abrupt* coolings only. The top frame compares the initial distribution of $\langle z_{\text{max}} \rangle_{\text{before}}$ with that after the cooling event, $\langle z_{\text{max}} \rangle_{\text{after}}$. The next frame shows the distribution of $\langle z_{\text{max}} \rangle_{\text{after}} < 3$ kpc for the abrupt coolings. The next frame shows the distribution of the ratios $\langle z_{\text{max}} \rangle_{\text{before}} / \langle z_{\text{max}} \rangle_{\text{after}}$ for this type of cooling. Finally, the bottom frame exhibits the evolution of the number of abrupt coolings binned in 0.5 Gyr bins.

The empirical probability of a halo particle to cool down to the disk plane and to remain within the disk at the end of the run is

$$f_{\text{cool}} = \frac{N_{\text{cool}}}{N_{\text{total}}} \quad (1)$$

where N_{cool} given by Figure 4. Results for both models are given in Table 1. $f_{\text{cool}} \sim 4.7\%$ in P00, and $f_{\text{cool}} \sim 2.9\%$ in P60.

The above results summarize the statistics of DM halo particles that experience the ‘cooling’ effect over various cooling intervals. To single out the extreme cooling effect, which proceeds over only 0.5 Gyr, we display the probability of such an *abrupt* event in Table 1. An example of such an abrupt cooling has been demonstrated in Figure 3a.

Observing the evolution of $N_{\text{cool}}(t)$ in the top frame of Figure 4, a trend emerges that it is correlated with the amplitude evolution of the stellar bar. In both P00 and P60 models, this number increases until the buckling, i.e., $t \sim 3$ Gyr in P00, and $t \sim 4$ Gyr in P60. After the buckling, the bar regrows in the P00 model until the end of the simulation, as is $N_{\text{cool}}(t)$. However, the remaining oval distortion in the P60 model after buckling (Figure 1) leads to a flattened $N_{\text{cool}}(t)$ in P60.

We now turn to estimate the cooling effect on the vertical *stellar* oscillation and supplement this with their radial migration for the halo stars in a full analogy with the DM halo particles. For this purpose, we assume that the halo stars have identical mass and are all metal-poor. Using, for example, the Chabrier (2003) initial mass function and the observed masses of metal-poor halo stars of $0.8 - 1 M_{\odot}$ (e.g., Valentini et al. 2019), we take the average stellar mass as $M_{\odot} \sim 1 M_{\odot}$ for simplicity. Note also that the statistics of cooled stars will be affected by replacing the DM particles used in the simulations by this average stellar mass.

In order to replace the DM particles by the stellar ones, we use the observations of the Milky Way stellar halo. Deason et al. (2019) estimated stellar mass of the MW stellar halo at $\sim 1.4 \times 10^9 M_{\odot}$. The density of stellar halo follows the power law of $\rho(r) \propto r^{-2.4}$ within ~ 17.2 kpc, and $\rho(r) \propto r^{-4.5}$ in the range $17.2 < r < 97.7$ kpc (e.g., Kafle et al. 2014).

Hence, the total stellar mass within the equipotential surface Φ_{max} in our model, and outside the disk with $|z| > 6$ kpc, corrected for including only the bound stars, can be estimated as $M_{*,\text{total}} \sim 1.3 \times 10^8 M_{\odot}$. Consequently, using the same cooling probability f_{cool} in eq. (1) for the halo stars as for the DM, we obtain $N_{*,\text{cool}} \sim 6 \times 10^6$ in the P00 model, and 4×10^6 in the P60 model (Table 1). To summarize, we expect the above $N_{*,\text{total}}$ residing in the contemporary MW disk.

Next, we analyze various kinematic parameters of the cooled stellar halo population, such as their radial migration and the ratio of prograde-to-retrograde orbits in the disk. We have measured $R(t)$ of these particles and calculated $\langle R_{\text{max}} \rangle$ the same way as $\langle z_{\text{max}} \rangle$. The resulting mean value of the distribution of their $\langle R_{\text{max}} \rangle$ is 9.4 kpc at $t = 0$ Gyr and 13.0 kpc at $t = 10$ Gyr, in the P00 model. For P60 model, the mean value of $\langle R_{\text{max}} \rangle$ is 9.7 kpc at $t = 0$ Gyr and 12.1 kpc at $t = 10$ Gyr. In comparison, the mean value of $\langle R_{\text{max}} \rangle$ of the entire sampled DM particles at $t = 0$ Gyr and $t = 10$ Gyr shifted from 9.5 to 11.0 kpc in the P00 model and from 9.5 to 9.9 kpc in P60 model (Fig. 6).

To obtain the ratio of prograde-to-retrograde orbits of the cooled stellar halo population, we assume that the halo stars kinematics follows that of the DM, which can be wrong for the P60 model when applied to the MW — the inner stellar MW halo discussed here has been found to be essentially nonrotating (e.g., Freeman 2012; Das et al. 2016; Deason et al. 2017). But because the properties of the inner stellar halos can be diverse, when applied to other galaxies, we still include this model. Under these conditions, we have calculated the averaged angular momentum over the last orbit before the end of the run (Figure 7). The prograde orbits are those spinning in the direction of the disk rotation. The resulting prograde-to-retrograde ratio of these particles is 1.2 : 1 in the P00 model and is 0.8 : 1 in the P60 model, when summed over all the cooled particles. However, these average ratios have little significance because the ratio depends on the radius, as we discuss below.

First, we find that the prograde and retrograde particles are distributed differently in the xy -plane at the end of the run (Fig. 8). In the P00 model, most of the prograde particles are distributed in a dumbbell shape with a major axis perpendicular to the major axis of the stellar bar. This dumbbell distribution reaches the radius beyond the bar size radius. In contrast, most retrograde particles dwell within the bar size radius and are distributed in an axisymmetric fashion. In the P60 model, with only an oval distortion at the end, the prograde particles have not shown any preferred azimuthal orientation. They are distributed more axisymmetrically than the prograde particles in the P00 model and extend to the region outside the bar size radius as well. The retrograde particles are distributed similarly to those in the P00 model. Most of them are within the bar size radius and distributed in an axisymmetric fashion.

Second, we checked the radial dependence of prograde-to-retrograde ratio (Fig. 9). Outside the bar-size radius, in the P00 model, this ratio increases monotonically and becomes larger than 10 outside the corotation radius. In the P60 model, this ratio is not monotonic but reaches $\sim 2 - 2.5$ outside the corotation, then drops to unity, following a substantial increase at larger radii. Therefore, faster spinning *stellar* halos produce a more shallow distribution of prograde-to-retrograde orbits outside the corotation.

Unfortunately, no data exists for the radial distribution of the prograde-to-retrograde ratio of metal-poor stellar population in the disk. Recent observations, which indicate this ratio being about 3:1 for Gaia DR3 (Bellazzini et al. 2023) and other samples (e.g., Reimers 1990; Beers et al. 1999; Starkenburg et al. 2017; Sestito et al. 2020; Lucey et al. 2021), may agree with both of our models. But detailed observations of the MW disk can provide the radial

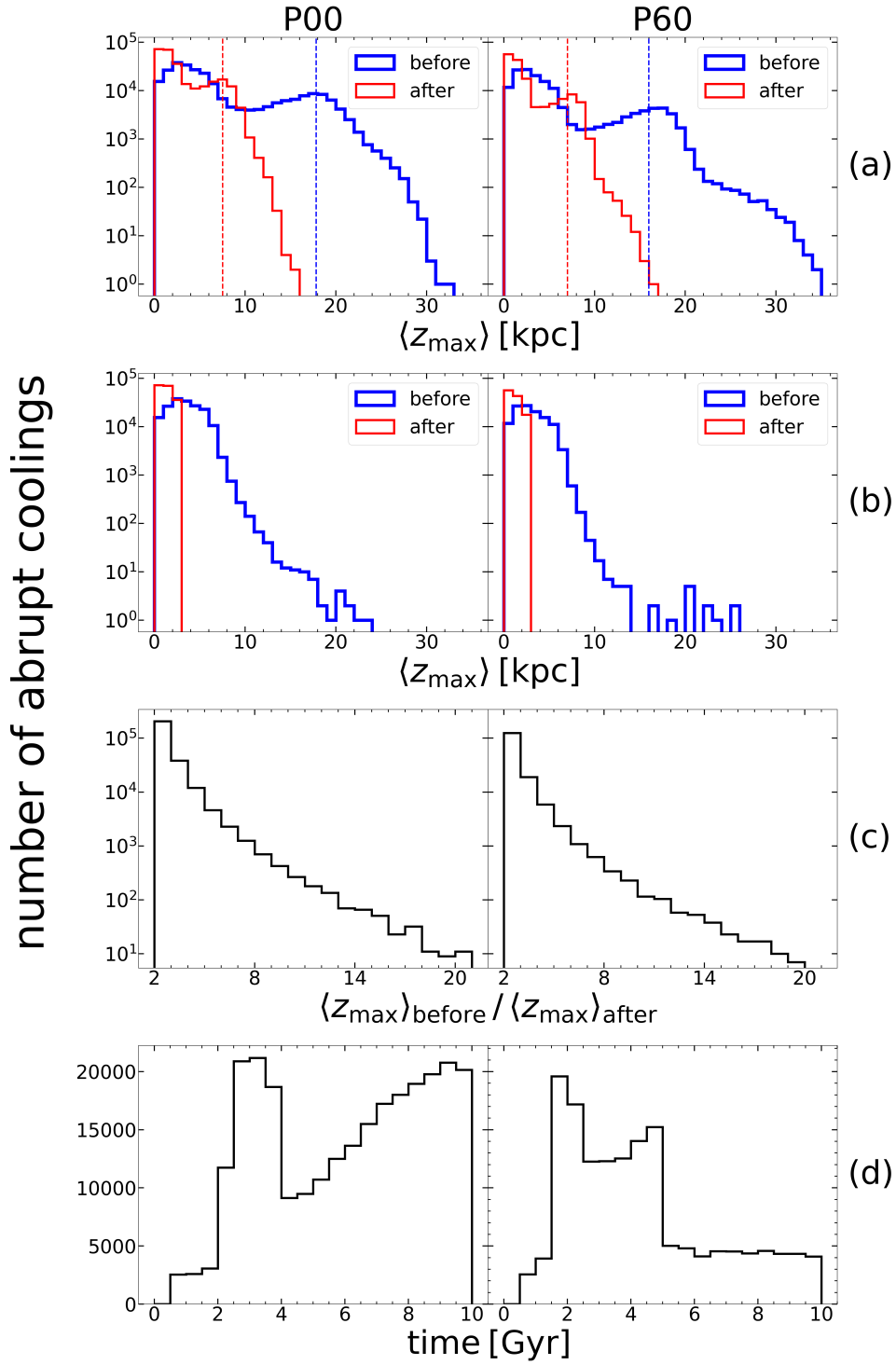


Figure 5. Additional statistics of $\langle z_{\max} \rangle$ for DM halo particles before and after each *abrupt* cooling, i.e., in ≤ 0.5 Gyr, with the P00 (left) and P60 (right). Here, by definition, $\langle z_{\max} \rangle_{\text{before}} / \langle z_{\max} \rangle_{\text{after}} > 2$. (a) Distribution of the number of abrupt coolings. The blue (orange) vertical dash line indicates the 90th percentile of $\langle z_{\max} \rangle_{\text{before}}$ ($\langle z_{\max} \rangle_{\text{after}}$) of abrupt coolings. The 90% of coolings lie to the left of the vertical lines. (b) Distribution of abrupt coolings with $\langle z_{\max} \rangle_{\text{after}} < 3$ kpc. (c) Distribution of $\langle z_{\max} \rangle_{\text{before}} / \langle z_{\max} \rangle_{\text{after}}$ of all abrupt coolings. (d) Evolution of the number of abrupt coolings in each time bin.

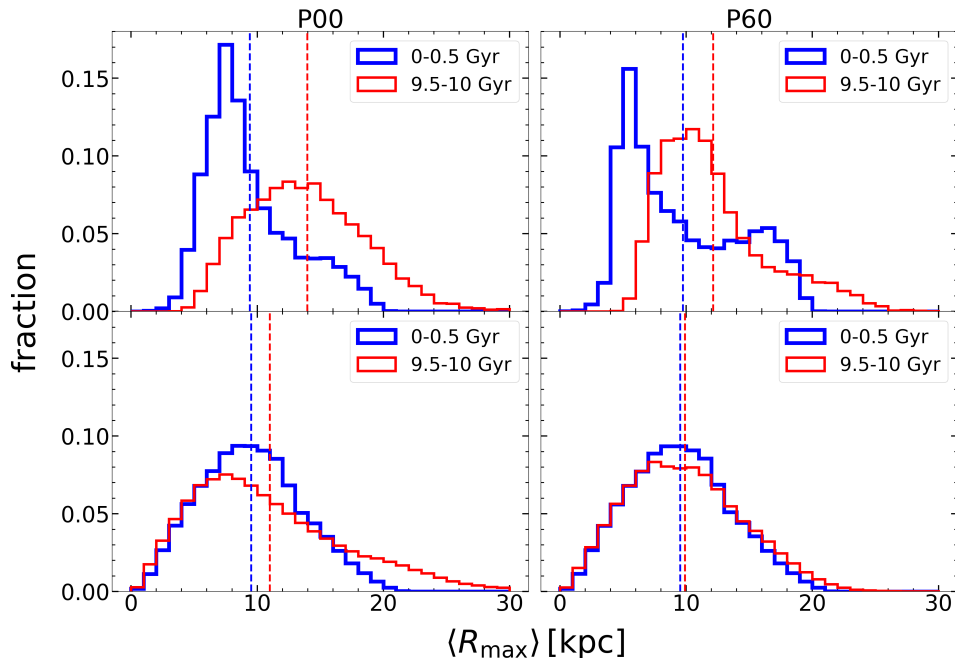


Figure 6. *Top:* The distribution function of $\langle R_{\max} \rangle$ from cooled particles of $N_{\text{cool}}(t = 10 \text{ Gyr})$ (see Figure 4). *Bottom:* Same as above, but for the entire sample. The vertical dashed lines show the average values for each distribution.

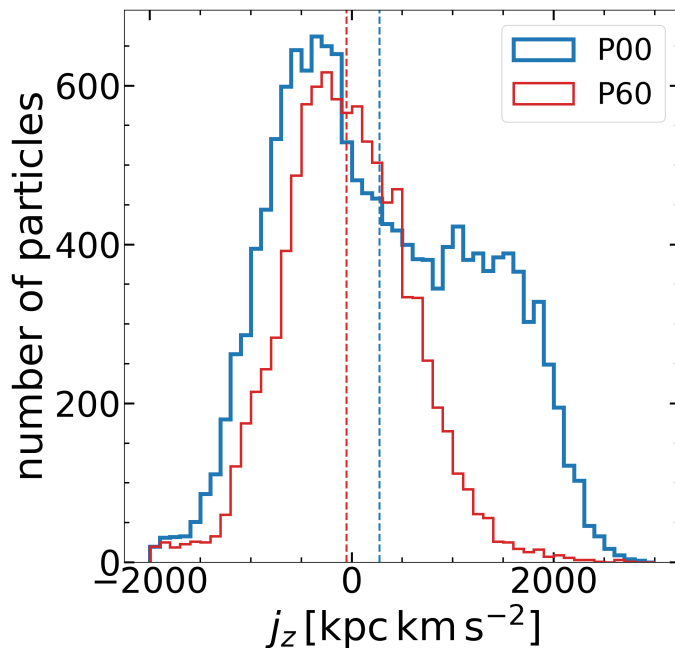


Figure 7. Distribution of the specific angular momentum, j_z , from cooled particles of $N_{\text{cool}}(t = 10 \text{ Gyr})$ (see Figure 4) for the P00 and P60 models. The vertical dashed lines show the average values for each distribution.

distribution of metal poor stars, and observations of other disk galaxies can reveal the scatter in this distribution which probably depends on the assembling history of their stellar halos.

In summary, we have presented a novel mechanism of cooling of the vertical oscillations of halo stars in barred disk galaxies with nonspinning and spinning DM halos. Using numerical simulations, we show that this mechanism is a resonant one where the vertical kinetic energy is absorbed by the stellar bar. This mechanism is also associated with the radial migration of metal-poor stars, which acquired disk kinematics and have corollaries to the chemical evolution

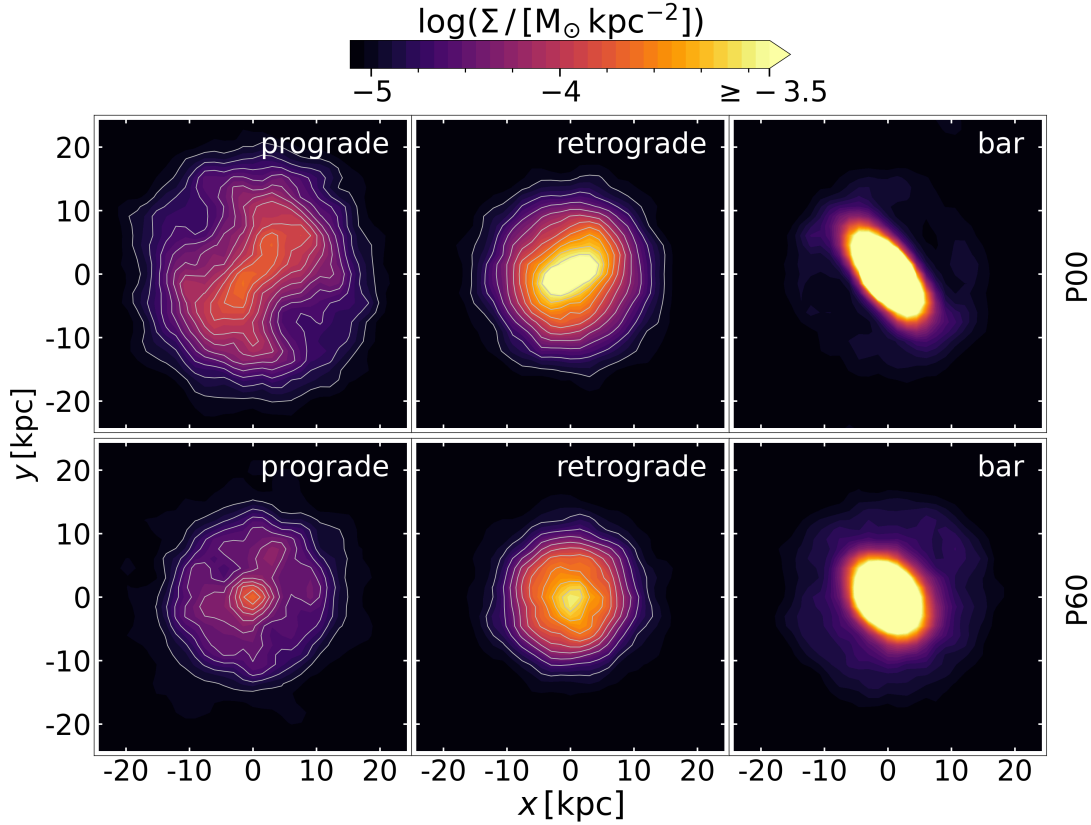


Figure 8. The distribution of cooled DM particles of $N_{\text{cool}}(t = 10 \text{ Gyr})$ (see Figure 4) in the x - y plane separated into prograde (left column) and retrograde (middle column) particles, for the P00 (top) and the P60 (bottom) models. The right column is part of randomly sampled disk particles showing the orientation of the stellar bar at the same time. The surface density of particles is plotted using contours with a linearly scaled color palette. The prograde and retrograde orbits have been identified by their instantaneous angular momentum J_z .

of disk galaxies. This cooling mechanism acts on a range of timescales, from a dynamical time of $\lesssim 0.5 \text{ Gyr}$ associated with 2–3 vertical oscillations to the secular timescale of a few Gyr. Using a typical MW stellar halo inferred from recent observations, we estimate the stellar metal-poor population in the contemporary MW disk contributed as a result of this new process. Furthermore, analyzing the kinematics of this disk population, we estimate the radial distribution of the prograde-to-retrograde orbits ratio for the metal poor disk population and find that the faster spinning stellar halo produces shallower distribution outside the corotation radius. More detailed numerical model comparison with the MW stellar halo properties can provide observational constrains on the stellar halo assembly.

- 1 We thank Phil Hopkins for providing us with the latest version of GIZMO, and to Da Bi for providing the data for
- 2 stellar halo from his cosmological simulations. I.S. is grateful for a generous support from the International Joint
- 3 Research Promotion Program at Osaka University. Simulations have been performed using the University of Kentucky
- 4 Lipscomb Computing Cluster. We thank Vikram Gazula at the Center for Computational Studies at the University
- 5 of Kentucky for help with the technical issues during the LCC runs.

REFERENCES

- Athanassoula, E. 2003, MNRAS, 341, 1179, doi: [10.1046/j.1365-8711.2003.06473.x](https://doi.org/10.1046/j.1365-8711.2003.06473.x)
- Athanassoula, E., Bienaymé, O., Martinet, L., & Pfenniger, D. 1983, A&A, 127, 349
- Beers, T. C., Rossi, S., Norris, J. E., Ryan, S. G., & Shefler, T. 1999, AJ, 117, 981, doi: [10.1086/300727](https://doi.org/10.1086/300727)

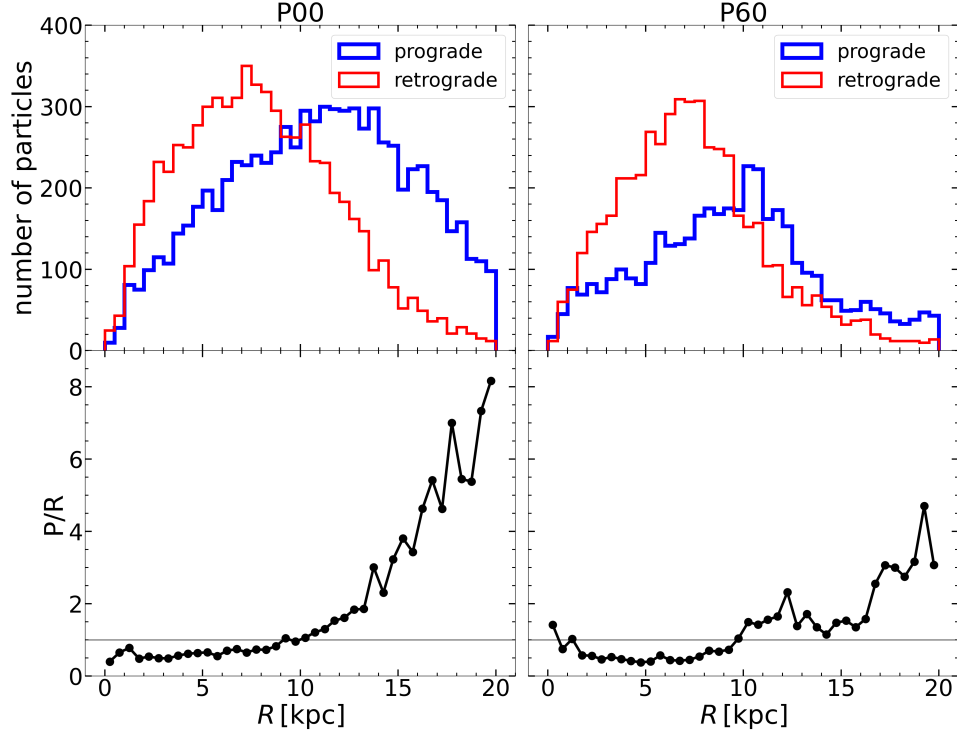


Figure 9. *Top:* Radial migration of cooled particle distribution for P00 (left) and P60 (right) models at $t = 10$ Gyr (the same population as in Figure 8). *Bottom:* Prograde-to-retrograde orbits ratio, P/R , as a function of radius for the P00 model (left frame) and P60 model (right frame) at $t = 10$ Gyr.

Bellazzini, M., Massari, D., Ceccarelli, E., et al. 2023, arXiv e-prints, arXiv:2312.02356, doi: [10.48550/arXiv.2312.02356](https://doi.org/10.48550/arXiv.2312.02356)

Bi, D., Shlosman, I., & Romano-Díaz, E. 2022, *ApJ*, 934, 52, doi: [10.3847/1538-4357/ac779b](https://doi.org/10.3847/1538-4357/ac779b)

Binney, J., & Tremaine, S. 2008, *Galactic Dynamics: Second Edition* (Princeton University Press, Princeton, NJ, USA)

Bullock, J. S., Dekel, A., Kolatt, T. S., et al. 2001, *ApJ*, 555, 240, doi: [10.1086/321477](https://doi.org/10.1086/321477)

Carollo, D., Christlieb, N., Tissera, P. B., & Sillero, E. 2023, *ApJ*, 946, 99, doi: [10.3847/1538-4357/acac25](https://doi.org/10.3847/1538-4357/acac25)

Chabrier, G. 2003, *PASP*, 115, 763, doi: [10.1086/376392](https://doi.org/10.1086/376392)

Collier, A., Shlosman, I., & Heller, C. 2018, *MNRAS*, 476, 1331, doi: [10.1093/mnras/sty270](https://doi.org/10.1093/mnras/sty270)

Combes, F., Debbasch, F., Friedli, D., & Pfenniger, D. 1990, *A&A*, 233, 82

Das, P., Williams, A., & Binney, J. 2016, *MNRAS*, 463, 3169, doi: [10.1093/mnras/stw2167](https://doi.org/10.1093/mnras/stw2167)

Deason, A. J., Belokurov, V., Koposov, S. E., et al. 2017, *MNRAS*, 470, 1259, doi: [10.1093/mnras/stx1301](https://doi.org/10.1093/mnras/stx1301)

Deason, A. J., Belokurov, V., & Sanders, J. L. 2019, *Monthly Notices of the Royal Astronomical Society*, 490, 3426, doi: [10.1093/mnras/stz2793](https://doi.org/10.1093/mnras/stz2793)

Di Matteo, P., Spite, M., Haywood, M., et al. 2020, *A&A*, 636, A115, doi: [10.1051/0004-6361/201937016](https://doi.org/10.1051/0004-6361/201937016)

Dubinski, J., Berentzen, I., & Shlosman, I. 2009, *ApJ*, 697, 293, doi: [10.1088/0004-637X/697/1/293](https://doi.org/10.1088/0004-637X/697/1/293)

Freeman, K. 2012, in *Astrophysics and Space Science Proceedings*, Vol. 26, Red Giants as Probes of the Structure and Evolution of the Milky Way, 137, doi: [10.1007/978-3-642-18418-5_14](https://doi.org/10.1007/978-3-642-18418-5_14)

Friedli, D., & Pfenniger, D. 1990, in *European Southern Observatory Conference and Workshop Proceedings*, Vol. 35, European Southern Observatory Conference and Workshop Proceedings, 265

Gaia Collaboration, Brown, A. G. A., Vallenari, A., et al. 2021, *A&A*, 650, C3, doi: [10.1051/0004-6361/202039657e](https://doi.org/10.1051/0004-6361/202039657e)

Hopkins, P. F. 2015, *MNRAS*, 450, 53, doi: [10.1093/mnras/stv195](https://doi.org/10.1093/mnras/stv195)

Jogee, S., Barazza, F. D., Rix, H.-W., et al. 2004, *ApJL*, 615, L105, doi: [10.1086/426138](https://doi.org/10.1086/426138)

Kafle, P. R., Sharma, S., Lewis, G. F., & Bland-Hawthorn, J. 2014, *The Astrophysical Journal*, 794, 59

Knapen, J. H., Shlosman, I., & Peletier, R. F. 2000, *ApJ*, 529, 93, doi: [10.1086/308266](https://doi.org/10.1086/308266)

Li, X., Shlosman, I., Heller, C., & Pfenniger, D. 2023b, *MNRAS*, 526, 1972, doi: [10.1093/mnras/stad2799](https://doi.org/10.1093/mnras/stad2799)

- Li, X., Shlosman, I., Pfenniger, D., & Heller, C. 2023a, MNRAS, 520, 1243, doi: [10.1093/mnras/stad076](https://doi.org/10.1093/mnras/stad076)
- Li, X., Shlosman, I., Pfenniger, D., & Heller, C. 2023c, Monthly Notices of the Royal Astronomical Society, 527, 11026, doi: [10.1093/mnras/stad3907](https://doi.org/10.1093/mnras/stad3907)
- Long, S., Shlosman, I., & Heller, C. 2014, ApJL, 783, L18, doi: [10.1088/2041-8205/783/1/L18](https://doi.org/10.1088/2041-8205/783/1/L18)
- Lucey, M., Hawkins, K., Ness, M., et al. 2021, MNRAS, 501, 5981, doi: [10.1093/mnras/stab003](https://doi.org/10.1093/mnras/stab003)
- Lynden-Bell, D. 1967, MNRAS, 136, 101, doi: [10.1093/mnras/136.1.101](https://doi.org/10.1093/mnras/136.1.101)
- Martinez-Valpuesta, I., Shlosman, I., & Heller, C. 2006, ApJ, 637, 214, doi: [10.1086/498338](https://doi.org/10.1086/498338)
- Navarro, J. F., Frenk, C. S., & White, S. D. M. 1996, ApJ, 462, 563, doi: [10.1086/177173](https://doi.org/10.1086/177173)
- Obreja, A., Buck, T., & Macciò, A. V. 2022, A&A, 657, A15, doi: [10.1051/0004-6361/202140983](https://doi.org/10.1051/0004-6361/202140983)
- Pfenniger, D. 1984, A&A, 134, 373
- Raha, N., Sellwood, J. A., James, R. A., & Kahn, F. D. 1991, Nature, 352, 411, doi: [10.1038/352411a0](https://doi.org/10.1038/352411a0)
- Reimers, D. 1990, The Messenger, 60, 13
- Sellwood, J. A. 1980, A&A, 89, 296
- Sellwood, J. A., & Wilkinson, A. 1993, Reports on Progress in Physics, 56, 173, doi: [10.1088/0034-4885/56/2/001](https://doi.org/10.1088/0034-4885/56/2/001)
- Sestito, F., Martin, N. F., Starkenburg, E., et al. 2020, MNRAS, 497, L7, doi: [10.1093/mnrasl/slaa022](https://doi.org/10.1093/mnrasl/slaa022)
- Sestito, F., Buck, T., Starkenburg, E., et al. 2021, MNRAS, 500, 3750, doi: [10.1093/mnras/staa3479](https://doi.org/10.1093/mnras/staa3479)
- Springel, V. 2005, MNRAS, 364, 1105, doi: [10.1111/j.1365-2966.2005.09655.x](https://doi.org/10.1111/j.1365-2966.2005.09655.x)
- Starkenburg, E., Martin, N., Youakim, K., et al. 2017, MNRAS, 471, 2587, doi: [10.1093/mnras/stx1068](https://doi.org/10.1093/mnras/stx1068)
- Valentini, M., Chiappini, C., Bossini, D., et al. 2019, Astronomy & Astrophysics, 627, A173
- Villa-Vargas, J., Shlosman, I., & Heller, C. 2009, ApJ, 707, 218, doi: [10.1088/0004-637X/707/1/218](https://doi.org/10.1088/0004-637X/707/1/218)
- Weinberg, M. D. 1985, MNRAS, 213, 451, doi: [10.1093/mnras/213.3.451](https://doi.org/10.1093/mnras/213.3.451)
- Yuan, Z., Li, C., Martin, N. F., et al. 2023, arXiv e-prints, arXiv:2311.08464, doi: [10.48550/arXiv.2311.08464](https://doi.org/10.48550/arXiv.2311.08464)
- Zhang, H., Ardern-Arentsen, A., & Belokurov, V. 2023, arXiv e-prints, arXiv:2311.09294, doi: [10.48550/arXiv.2311.09294](https://doi.org/10.48550/arXiv.2311.09294)